https://africanjournalofbiomedicalresearch.com/index.php/AJBR
Afr. J. Biomed. Res. Vol. 27 (October 2024); 805- 822
Research Article

Hybrid Deep Learning Algorithm for Multi-Grade Brain Tumor Classification

Kondra Pranitha[1*], Naresh Vurukonda[2*]

[1]Research Scholar, Department of CSE, Koneru Lakshmaiah Education Foundation, Vaddeswaram, AP, 522302, India.*
[2]Department of CSE, Koneru Lakshmaiah Education Foundation, Vaddeswaram, AP, 522302, India.*
naresh.vurukonda@kluniversity.in

Abstract
One of the potentially fatal conditions impacting a person's general health and brain function is a brain tumor. Early-stage brain tumor identification and classification accuracy is critical to saving lives. One of the most popular methods used in the medical field to classify brain tumors is deep learning. Nevertheless, current deep learning methods are insufficiently effective in precisely categorizing the various stages of brain cancers. In this study, Ensemble Learning with Deep Convolutional Long Short-Term Memory (EL-DCLSTM) was proposed to categorize multiple grades of brain tumors accurately. The first step in the suggested methodology is the acquisition and preparation of brain MRI data. As a result, the enhanced U-Net method was used for the segmentation stage in order to extract the region of interest from the previously processed images. In addition, the Firefly-optimized ResNet architecture was used for feature extraction, which involved selecting and extracting the most pertinent features for classifier training from the segmented images. The suggested EL-DCLSTM was applied for brain tumor classification after feature extraction. The system can accurately manage fluctuations in MRI data thanks to the DCLSTM design, which combines the effectiveness of convolutional and LSTM layers for capturing both spatial and temporal properties in the MRI images. However, ensemble learning generates the final classification results by aggregating the predictions from individual DCLSTM models that were trained on the extracted feature set's feature subsets. The suggested approach obtained better accuracy of 0.98172 and 0.99138 for 70% and 80% training ratios, according to the experimental results.

Keywords: Deep Learning, Brain tumor classification, Firefly optimization, Feature extraction, Segmentation

***Author for correspondence:** *naresh.vurukonda@kluniversity.in*

Received: 30 September 2024. Accepted: 16 October, 2024.

DOI: https://doi.org/10.53555/AJBR.v27i3.2974

Introduction

Nowadays, brain tumors are among the most dangerous illnesses that impact millions of individuals globally. [1]. The aggregate properties of the aberrant brain cells are the main cause of brain tumors. Brain tumors usually progress through two stages: primary and secondary. [2]. Because the tumor is small at the first stage, it is referred to as "benign" in biology. However, in the secondary stage, the tumors grow larger and begin to spread to other parts of the body. In terms of biology, this stage is called "malignant." According to a study by the National Brain Tumor Society of the United States of America (USA), brain tumor disease affects about 700,000 people. [3]. Of these, malignant disorders affect the remaining 69.8% of cases, which are benign. The fact that just 36% of the patients survived was brought to light in this report. Additionally, it showed that the number of people affected by brain tumors rose from 87,000 in 2020 to 84,170 in 2021. [4]. Furthermore, it was noted that persons over 40 experience the majority of these causes (69,950). The brain tumor is further classified into two stages, High-Grade Glioma (HGG) and Low-Grade Glioma

(LGG), in accordance with the high death rate. It should be mentioned that the survival rate of LGG is higher than that of HGG. [5]. On the other hand, the patients' ability to survive brain tumors is contingent upon prompt and dependable therapy. The clinical community treats brain tumors at different stages using a variety of techniques. In the primary stage, radiography is routinely used by healthcare practitioners to help patients survive without surgery. [6]. As a result, clinical professionals frequently use radiography and chemotherapy to treat the secondary or malignant stage. [7]. However, appropriate treatment planning depends on the early and correct diagnosis of malignancies. Medical professionals currently use imaging technology extensively to identify and categorize cancers, such as skin cancer, stomach cancer, brain tumors, and blood cancer. [8, 9]. Imaging methods like Computed Tomography (CT) and Magnetic Resonance Imaging (MRI) are employed for the classification of brain cancers.[10]. However, the studies found that MRI pictures are more useful for classifying brain tumors than CT scans. Computer-aided diagnostic (CAD) systems have become widely employed in medicine in recent years to automatically detect and classify brain cancers in their early stages. [11, 12]. A number of processes are involved in the CAD system, such as feature engineering, feature reduction, picture preprocessing, and classification utilizing supervised algorithms. [13]. The preprocessing models improve the quality of the images and eliminate noisy features. The salient features, such as texture, shape, etc., are recorded during the feature extraction stage. [14, 15]. The dimensionality of the pictures is decreased in the feature reduction step, and the tumors are then categorized using supervised algorithms such as Support Vector Machine (SVM), Naive Bayes (NV), and K-Nearest Neighbor (KNN). [16, 17]. However, the CAD systems are unsuitable for multiclass classification problems [18]. Deep learning (DL) has been introduced into the medical area, and this has led to improved outcomes for classification tasks, especially multiclass classification. [19]. In multiclass classification, the DL models—Deep Neural Networks (DNN), Artificial Neural Networks (ANN), Convolutional Neural Networks (CNN), etc.—have demonstrated superior accuracy when compared to the CAD systems. [20]. Even while DL models are more accurate, they have drawbacks such as poor interpretability, overfitting, poor generalization, high processing resource requirements, long calculation times, and limited scalability. [21]. In order to develop an automatic detection and classification model for brain tumor analysis in the medical industry, it is imperative that these concerns be addressed. To solve these problems, a hybrid DL model was presented in this study. The following is a description of the study's principal contributions.

- To achieve increased segmentation, the proposed framework makes use of an updated version of the U-Net technique, which allows it to extract the region of interest from the input images.
- The created framework uses a ResNet architecture that has been tuned for Firefly as a feature extractor, allowing the system to extract the most significant and informative features for classification.
- This study combines Deep Convolutional Long Short-Term Memory and Ensemble Learning to create a hybrid deep learning technique for multiclass brain tumor classification.
- Ultimately, the suggested approach was contrasted and verified against the current models in terms of accuracy, precision, recall, f-measure, false positive rate, and so on.

Section 2 of the presented study outlines the comprehensive review of previous research, followed by the problem statement in Section 3, the methodology in Section 4, the results and comparative analysis in Section 5, and the article conclusion in Section 6.

Related works

The following is a description of a few recent works related to the classification of brain tumors.One of the fatal illnesses that impact millions of individuals globally is brain tumors. Accurately identifying and classifying this fatal illness is essential for effective treatment planning and raising survival rates. Milica M. Badža et al. [22] used a CNN architecture for the detection and categorization of three different kinds of brain cancers. This framework is validated on T1-weighted contrast-improved MRI data, and its design is akin to the pre-trained networks'. Furthermore, subject-wise cross-validation and 10-fold cross-validation were used to verify the generalization effectiveness of this technique. The results of the implementation showed that this method reached 96.56% with faster execution. Nevertheless, the interpretability of this study is lacking, which restricts its use in actual clinical settings.

Ayesha Jabbar et al. [23] suggested the use of a hybrid deep learning model to create an automatic brain tumor classification method. CapsNet, or the capsule neural network, and VGGNet are combined in this hybrid method. This work aims to alleviate the problem of massive data requirements that come with deep learning for tumor classification. We assessed this proposed methodology with the Brats-2020 and Brats-2019 databases. This methodology obtained 0.99% accuracy, 0.98% sensitivity, and 0.99 specificity, as confirmed by the experimental data. Nevertheless, there are issues with this approach, namely its high complexity and restricted generalizability.

Muhammad Imran Sharif et al. [24] created an automated deep learning approach to classify brain cancers into multiple classes. A refined Densenet201 Pre-Trained DL framework was created for feature engineering in this study. Additionally, a modified evolutionary algorithm and entropy-Kurtosis-based high feature values were employed as feature selection methods. Lastly, for tumor classification, a Support Vector Machine (SVM) cubic classifier was used. The BRATS2018 and BRATS2019 databases saw an accuracy of 95% on average because to this cooperative approach. But this approach takes longer to train, which limits how well it works in practical situations.

Sandeep Kumar et al. [25] investigation to create a precise method for classifying brain tumors using MRIs. In order to distinguish between benign and malignant MRI images, this study changed the traditional CNN model by using the transfer learning algorithm (an enhanced version of ResNet-50).

According to the experimental data, this technique achieved a 96.40% malignant classification accuracy and a 97.23% benign classification accuracy. Additionally, this study's validation across a number of pre-trained models showed that the enhanced method provided higher accuracy. However, the effectiveness of this method depends on the quality of the training data.

Sohaib Asif et al. [26] offered a framework for deep transfer learning to speed up the categorization of brain tumors. Five well-known DL architectures were used in this work: Xception, DenseNet201, DenseNet121, ResNet152V2, and InceptionResNetV2. To improve the accuracy of the model, a deep, dense block and softmax layer were added to the final layer of this framework. Two databases were utilized to validate this research. There are three classes in the first dataset and four classes in the second. According to the implementation findings, this technique achieved accuracy rates of 96.67% and 95.87% for the two datasets. This tactic, though, is unable to adjust to the changing circumstances.

Marwa M. Emam et al. [27] offered a framework that is optimized for the problem of classifying brain tumors. For effective learning and classification, this methodology combined the meta-heuristic optimization algorithm with DL architecture. To increase accuracy, this algorithm coupled the residual learning model's features with those of the Improved Hunger Games Search algorithm. Using the three brain MRI image datasets, this methodology was trained and validated and compared to industry benchmarks such as MobileNet, ResNet-50, and DenseNet201. According to the testing results, this strategy's accuracy was 97.23%, 97.33%, and 99.41%, in that order. However, this approach requires a lot of work and uses more resources. Furthermore, the interpretability of this method is lacking, which restricts its use in actual clinical settings.

Sadafossadat Tabatabaei et al. [28] combined many DL architectures, such as the Transformer model, self-attention network, and CNN, to create a two-branch parallel framework that accurately predicted the tumor classes. Furthermore, a simplified and improved CNN model was created to distinguish tumor characteristics from MRI pictures. With 3064 samples in the brain MRI image dataset, this framework was tested and shown to have 97.59% accuracy. Furthermore, in comparison to current models, this methodology delivers fast and accurate diagnosis. However, there are significant memory and processing power requirements when using attention modules.

Hossein Mehnatkesh et al. [29] presented a deep convolutional ResNet model that has been developed for accurate and quick tumor prediction using MRI scans. This approach combines the traditional DCNN model with the features of Modified Ant Colony Optimization. The system can achieve faster convergence and prevent local optima because to this integration. According to the implementation findings, this approach achieved 0.9764 accuracy with a reduced computing time. This method, however, is inappropriate for datasets that are unbalanced.

System Model and Problem Statement

One of the deadliest illnesses that impact many people globally are brain tumors. Precise and prompt diagnosis is essential for efficient treatment planning and a higher patient survival rate. On the other hand, this disease's classification and prediction are difficult and time-consuming. As a result, multiple building pieces are created for AI-based tumor classification models, including data processing and collecting, feature engineering, classification, and interpretation. Patient samples are gathered and preprocessed in the first block.

On the other hand, the most illuminating characteristics that distinguish between the tumor and non-tumor groups are identified and retrieved in the second block. The model is trained with the data in the classification block to comprehend the patterns and architectures of tumors. In the interpretation block, the categorization findings are finally assessed and severity rates are looked at.

While AI-based models are more efficient, there are still several issues that need to be resolved before they can be used in practical situations. A restricted generalization and a high likelihood of overfitting are the main drawbacks. [30]. They often get overtrained on the training samples and lack the efficiency to predict tumors on unseen or new samples. The second challenge is the limited accuracy and high false positive rate in multiclass classification tasks. Thirdly, the existing models demand more computational resources, including memory, processing power, and large training data for effective functioning. In addition, one of AI models' intrinsic challenges is their lack of interpretability, which makes it challenging and complex for medical experts to comprehend the rationale behind the prediction. This paper developed a hybrid deep learning architecture that leverages the advantages of DCLSTM and ensemble learning to overcome these issues.

Proposed EL-DCLSTM Methodology for Brain Tumor Classification

A hybrid EL-DCLSTM algorithm was created to precisely identify and categorize different types of brain tumors. The patients' MRI scans were used in this work to train the model to recognize and comprehend the patterns of different tumor types. First, preparation operations are carried out in order to normalize the images for later procedures. As a result, enhanced U-Net and ResNet algorithms are used for segmentation and feature extraction. Ultimately, the suggested classifier was used to classify brain tumors. Figure 1 shows the suggested approach.

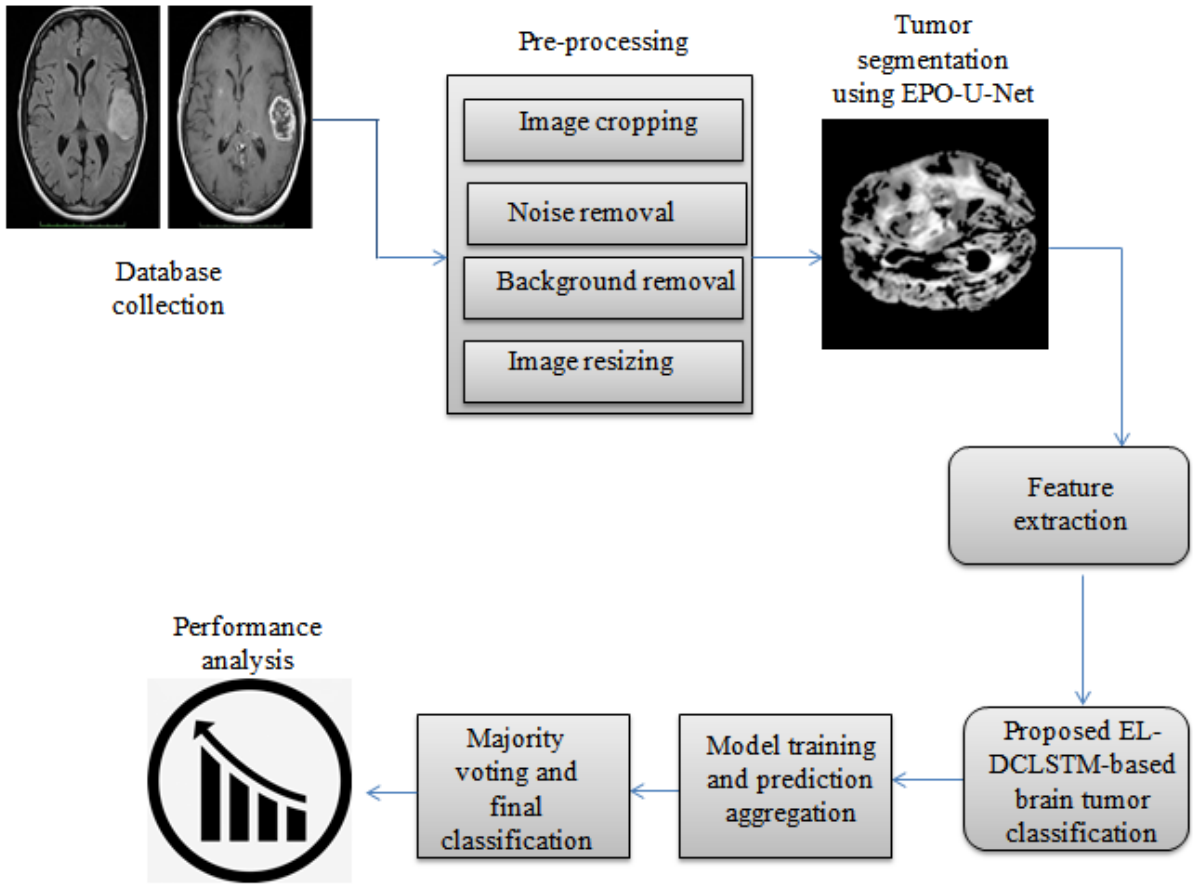

Figure 1: Proposed EL-DCLSTM framework

Data collection

First, in a medical setting, MRI samples are taken from both healthy individuals and those with brain tumors. The model is trained using a database created by combining and labeling all of the gathered photos. This created database includes classes for both normal and distinct brain tumors. The BraTs 2020 database [31], which is made up of routine clinically collected preoperative multimodal MRI scans from multiple institutions, was used in this investigation. It includes scans of lower grade glioma (LGG) and glioblastoma (GBM/HGG), along with accessible overall survival (OS) statistics and a pathologically confirmed diagnosis.

The T2-weighted (T2), native (T1), post-contrast T1-weighted (T1Gd), and T2 Fluid Attenuated Inversion Recovery (T2-FLAIR) volumes make up the dataset. One to four raters manually separate each image into various tumor sub-regions, such as the necrotic and non-enhancing tumor core (NCR/NET), peritumoral edema (ED), and GD-enhancing tumor (ET).

Image preprocessing

One of the most important steps in the tumor classification process is image preparation. By using a series of sets on the raw dataset, this phase attempted to improve the quality of the MRI pictures for processing in the future. Image resizing, background removal, cropping, and filtering (noise removal) are the procedures involved. All of the database's photographs are cropped in the image cropping stage by eliminating any undesired regions. This stage aids in the suggested system's ability to concentrate more on regions of interest (ROI) than undesirable areas. Gaussian filtering was used in the noise removal stage to get rid of the noise features from the cropped MRI pictures.Noises are the random variations in the visual signal that can be brought about by a variety of issues, such as inadequate illumination, subpar imaging equipment, etc. The developed technique removed the random noises from the cropped photos by applying Gaussian filtering. By computing the average value of the surrounding pixels using the Gaussian distribution, this filtering algorithm replaces the noisy pixel in the image. The Gaussian filtering is mathematically represented in Eqn. (1).

$$G_f(x,y) = I(x,y) * \frac{1}{2\pi\sigma^2} e^{-\frac{x^2+y^2}{2\sigma^2}} \quad (1)$$

Where $I(x,y)$ represents the input MRI image, $G_f(x,y)$ defines the filtered image, (x,y) indicates the kernel coordinates, and σ denotes the standard deviation of the Gaussian distribution. As a result, image thresholding was used to separate the filtered images from the background. Finally, to guarantee consistency across all the photos in the collection, bicubic interpolation was used to resize the photographs into a specific size. Along with these actions, data augmentation procedures including rotation, scaling, flipping, scaling, and

shearing are carried out to provide diversity to the training set and address the overfitting issues with the model.

Image segmentation

The technique of removing ROIs from previously processed MRI scans is known as image segmentation. The preprocessed image is divided into several regions, each of which represents a different area of the image [32]. This phase speeds up image processing and improves classification accuracy. The produced work used an upgraded U-Net architecture for picture segmentation. By integrating EPO's optimization power into the traditional U-Net architecture, this method enables the system to segment data by iteratively improving training parameters like bias and weights.

Three components make up the traditional U-Net structure: the encoder, bottleneck, and decoder. After receiving the preprocessed images, the encoder module uses dense convolution and pooling processes to downsample the images. With this technique, the significant spatial features are preserved while the image size is decreased. The bottleneck receives these reduced-resolution photos. A Deep Neural Network (DNN) technique is included in this component, which uses the downsampled images to extract high-level feature representation.

Lastly, the decoder does a deconvolution operation to upsample the picture that was taken from the bottleneck. The result of segmentation is the upsampled image. Emperor Penguin Optimization (EPO), which optimizes the model parameters of the U-Net method, such as weights, neurons, bias, etc., was used to improve the algorithm's performance. This connection enhances picture segmentation transparency in addition to training. The segmentation and preprocessed images are shown in Figure 2.

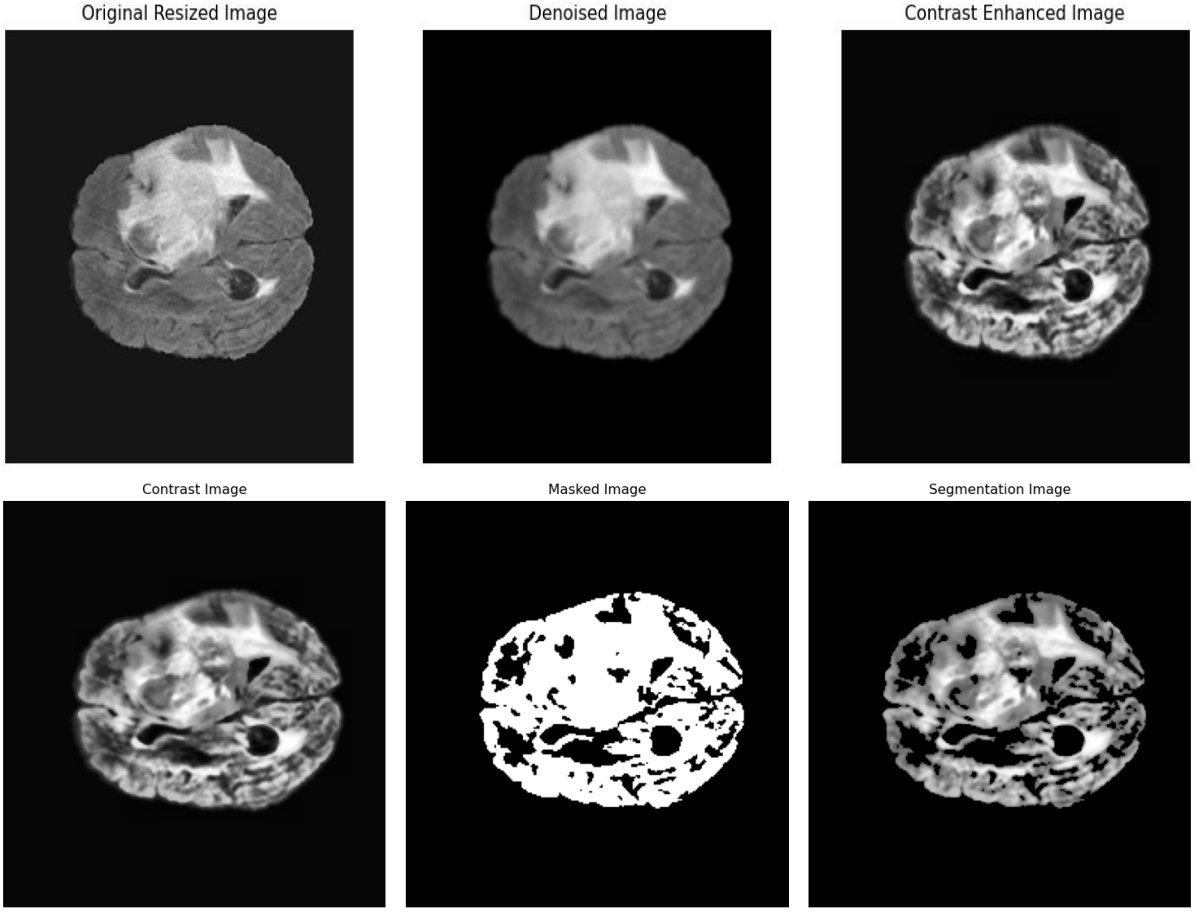

Figure 2: Preprocessed and segmented images

The EPO is an optimization algorithm inspired by nature that solves a variety of optimization problems by modeling the communal huddling behavior of emperor penguins. By thoroughly examining the search space, this method seeks to determine the U-Net model's ideal value. The initial hyperparameter values are entered into this procedure, which randomly initializes them. This led to the definition of an objective function to ascertain the fitness value for every hyperparameter sequence. The objective is to minimize the cross-entropy loss incurred by the U-Net model, represented in Eqn. (2).

$$L_o(c,c') = -\sum_{i=1}^{n} c'(i)\log(c(i)) \quad (2)$$

Where $L_o(c,c')$ indicates the loss function, $c'(i)$ represents the probability of the class, and $c(i)$ defines the predicted probability of the class produced by the model. The objective function was utilized to ascertain the fitness value of every

potential solution. A greater fitness value is obtained by the solution with less loss, whereas a lower fitness value is obtained by the solution with more loss. After then, the population was sorted in descending order to find the best possible candidate answer. Finally, the system explores the search space and updates the parameter values using Eqn. (3).

$$p(t+1) = p(t) - \vec{q}.p^{*}(t) \quad (3)$$

Where $p(t+1)$ indicates the updated parameter set, $p(t)$ represents the current parameter set, $p^{*}(t)$ defines the best solution at iteration *t*, and $\vec{q}$ denotes the factor preventing collision in exploration. Further, the solution with higher fitness was selected for U-Net training.

Feature extraction

Feature extraction is the process of identifying and removing the essential characteristics needed to differentiate between the various types of brain tumors [33]. The system's goal in this module is to recognize important characteristics such as area, direction, color, form, intensity, texture, size, and edges. The suggested study combined the ResNet algorithm with firefly optimization to build a hybrid feature extractor. A CNN model that has already been trained, the ResNet method has a higher chance of identifying high-level features. The convolution operations in this model are carried out by numerous convolution layers, which also extract the feature sequence from the segmented images. Here, the five convolutional layers of the ResNet-50 architecture were used.

A max-pooling layer with a filter size of [3x3] comes after the first convolution layer, which has 64 kernels with dimensions of [7x7x3]. In order to place four convolution layers, the kernel is increased from 64 to 2018. There are residual blocks of various dimensions in each convolution layer: [1x1], [3x3], and [1x1]. Ultimately, the extracted feature sequence was provided by a completely linked layer that was positioned. The firefly optimizer (FO), using its optimization skills, selects the features (most informative attributes) for DCLSTM training based on the extracted feature set. This algorithm works by initializing features similar to the firefly population in the FO algorithm, represented in Eqn. (4)

$$f_{st} = \left\lfloor fe_1, fe_2, fe_3, ..., fe_p \right\rfloor \quad (4)$$

Where f_{st} defines the final extracted feature sequence and fe_1 the feature vector extracted from the image. When choosing features, the FO takes into account how important it is to distinguish between various tumor classes. As a result, features with similar information were eliminated based on appeal. Then, the FO explores the search space to find the optimal feature sequence mathematically represented in Eqn. (5).

$$fe_i(t+1) = fe_i(t) + \hbar\, e^{-A_{tr}\left(fe_i, fe_j\right)}\left(fe_i - fe_j\right) + \beta \quad (5)$$

Where β indicates the randomness and $fe_i(t+1)$ indicates the updated feature. The features with attractiveness less than 0.5 are chosen for model training once the feature sequence has been updated. This mechanism is iterative in nature and keeps going until the maximum iteration or convergence rate is achieved. With each iteration, this approach generates a new feature sequence for the classifier unit.

Brain tumor classification

Classifying brain tumors involves identifying patterns among the various tumor classes. In this case, the suggested EL-DCLSTM algorithm was used [34]. Three distinct deep learning architectures—ensemble learning, deep convolutional neural networks, and long short-term memory (LSTM)—are combined in the suggested model. In order to forecast the various tumor types, we first integrate the DCNN with the LSTM module, which has been trained using the retrieved feature sequences. An input layer, convolutional layer, pooling layer, LSTM layer, fully connected layer, and output layer are all present in the integrated DCLSTM module. The convolutional layers apply filters (kernel) and capture the spatial information from the MRI images, which are crucial for differentiating the different tumor classes. These layers form a feature map, which highlights the local patterns and correlations within the images, and it is mathematically presented in Eqn. (7).

$$Fm(x,y) = \sum_{v}\sum_{u} P_i(x+v, y+u).kf(v,u) \quad (7)$$

Where $Fm(x,y)$ represents the value of the created feature map at position (x, y), $P_i(x+v, y+u)$ denotes the input image pixel value at location, and $kf(v,u)$ indicates the filter weight at position. An activation function called the Rectified Linear Unit (ReLU) comes after this layer. It adds non-linearity and aids in the analysis of complicated and complex patterns. In order to reduce the feature map's spatial dimensions, a pooling layer was added after the activation function. This layer removes the unwanted features while preserving the most informative spatial information from the images represented in Eqn. (8).

$$Fm_{pl}(x,y) = \max_{v,v} Fm\ (x \times W + v, y \times W + u) \quad (8)$$

Where $Fm_{pl}(x,y)$ defines the values of the input feature map covered by the pooling window W and $Fm\ (x \times W + v, y \times W + u)$ represents the value of the input feature sequence at the location $(x \times W + v, y \times W + u)$. Among the many gates and states present in the LSTM layers are the input gate, forget gate, output gate, memory cell, and hidden states. The input gate's job is to regulate the flow of data into the memory cell.

[35]. The forget gate is responsible for restricting the amount of unwanted content that can be accessed by removing it. The memory cell state functions as the long-term memory of the module by storing important data or information from the input. Relationships, patterns, and other noteworthy traits that distinguish the different tumor classifications make up the important data. The LSTM layer is mathematically modeled using Eqn. (9), (10), (11), (12), and (13).

$$Ip_t^{g} = \sigma\left(\lambda_t^{ig}.\left[Hi_{t-1}.I_t\right] + \gamma_t^{ig}\right) \quad (9)$$

$$Fo_t^g = \sigma\left(\lambda_t^{fg}.\left[Hi_{t-1}.I_t\right] + \gamma_t^{fg}\right) \quad (10)$$

$$Op_t^g = \sigma\left(\lambda_t^{og}.\left[Hi_{t-1}.I_t\right] + \gamma_t^{og}\right) \quad (11)$$

$$Cs_t^s = \tanh\left(\lambda_t^c.\left[Hi_{t-1}.I_t\right] + \gamma_t^c\right) \quad (12)$$

$$Hi_t = Op_t * \tanh\left(Cs_t^s\right) \quad (13)$$

Where $\tanh$ indicates the hyperbolic tangent activation function, σ defines the sigmoid activation function, Ip_t^g, Fo_t^g, Op_t^g represents the input gate, forget gate, and output gate, Cs_t^s indicates the memory cell state, Hi_t refers to the hidden state, λ defines the weight matrices, and γ represents the bias vector. These gates and states aid in the long-term storage and analysis of data by controlling the flow of information. The MRI scans' temporal information and long-term dependencies, as well as the tumor features and their variation, are all interpreted by the system using this process. These layers extract temporal and spatial information from the MRI scans, which enables it to discriminate between different tumor categories. Several convolutional, pooling, and LSTM layers were followed by the addition of a fully linked layer. This layer transforms the feature map into a hierarchical feature representation, and its outcome is expressed in Eqn. (14).

$$Fc = \sigma.\left(Fst.\lambda + \gamma\right) \quad (14)$$

where λ defines the weight matrix, Fst indicates the feature map, and γ represents the bias vector. The output layer receives this outcome and uses it to conduct categorization. The input image features are mapped into the appropriate classes by the output layer.

The study that was presented combined DCLSTM with ensemble learning based on majority voting to determine final classifications. In ensemble learning, several models' classifications or predictions are combined to produce a final forecast that is both accurate and dependable. The models in the majority voting-based ensemble model are trained with the dataset and asked to cast their votes for the prediction's outcome at that moment. [36]. The final projections are estimated by the majority's choice. The training phase, the categorization phase, and the decision-making phase are the three stages of this process. During the training phase, several DCLSTM models with various hyperparameter values are produced. To classify tumors, each model will be trained using subsets of extracted feature sequences. During the classification stage, each trained model received the fresh MRI picture as input. Every model independently classifies data according to the patterns and knowledge they have acquired. A specific class name will be the outcome of this classification. Every forecast is regarded as a vote in favor of the particular class label. Finally, in the decision-making phase, all classification results are collected from multiple DCLSTM models, and a majority voting mechanism is applied to produce final classification results, expressed in Eqn. (15).

$$Fp_I = \underset{tc\in\{tc1,tc2,\ldots,tc_n\}}{\arg\max} \sum_{i=1}^{s} Ic\left(pr_i\left(I\right) = tc\right) \quad (15)$$

Where Fp_I indicates the final classification results, tc represents the tumor classes available in the dataset, Ic defines the indicator function, and $pr_i(I)$ defines the classifications made by individual DCLSTM models. The class name with the most votes is returned by the arg max function, and the class's vote total is counted by the indicator function.

The indicator function is defined in Eqn. (16).

$$Ic\left(pr_i\left(I\right) = tc\right) = \begin{cases} 1; if \;\; pr_i\left(I\right) = tc \\ 0; otherwise \end{cases} \quad (16)$$

This indicator function adds the votes for each class. In case the DCLSTM model assigns a classification of "0" for class "0," it is seen as a vote in favor of class "0." All classes are subject to this counting procedure, and the class with the greatest number of votes receives the final classification. As a result, the system is able to investigate several models and raises the classification accuracy overall. Additionally, it aids in reducing uncertainty in prediction outcomes, improving its effectiveness and dependability in tumor classification. The suggested strategy's flowchart is shown in Figure 3. Algorithm 1 presents the developed algorithm's operation in pseudocode language.

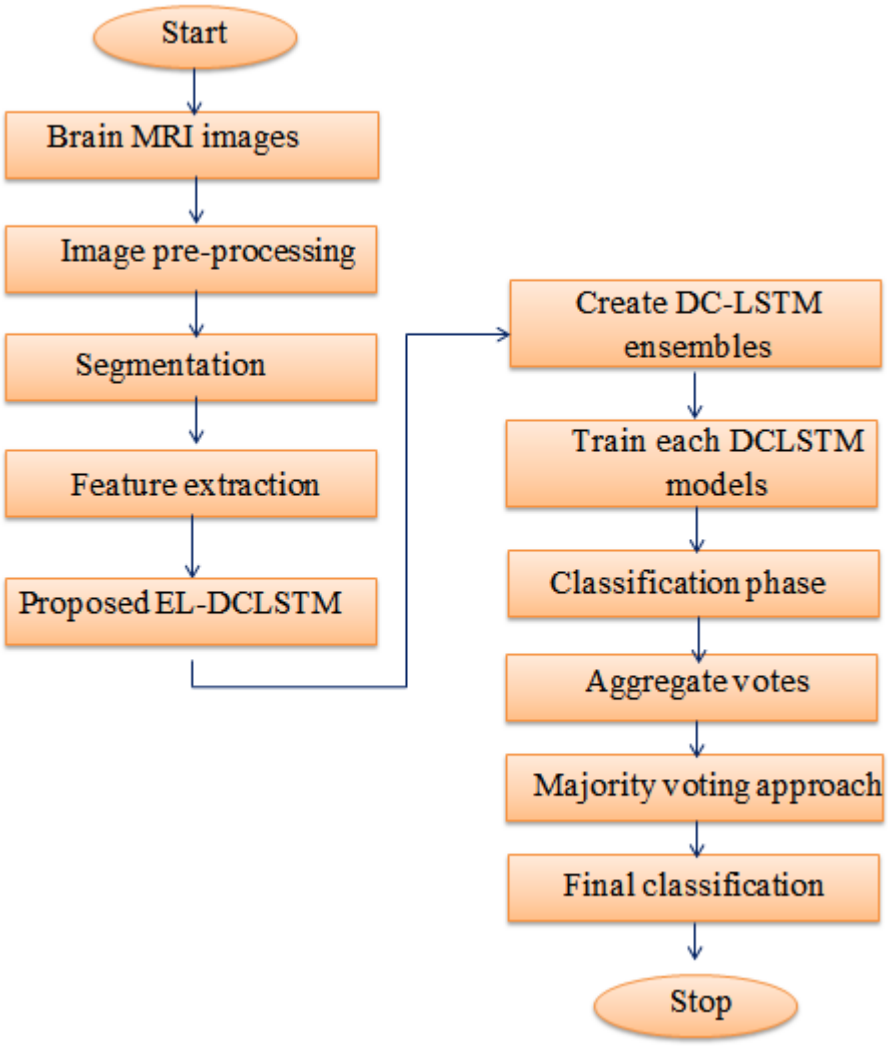

Figure 3: Flowchart of the proposed strategy

Algorithm: EL-DCLSTM
Input: Brain MRI images, number of DCLSTM model, iteration count, DCLSTM hyperparameters;
Output: Tumor class;
Initialization: Initialize images and other inputs;
1. Data preprocessing:
For each image:
Apply image cropping;
Apply Gaussian filter to remove noises;
Apply thresholding to eliminate background;
Resize the image using bicubic interpolation;
End for;
2. Data augmentation;
3. Image segmentation:
For each image in the database:
Encode the image using a U-Net encoder;
Extract high-level features using DNN in the bottleneck;
Decode the image using a U-Net decoder;
Optimize U-Net parameters using EPO;
End for;
4. Feature extraction:
For each segmented image:

Extract initial features using ResNet-50;
Apply firefly optimization for feature selection;
Explore and select features with attractiveness less than 0.5;
End for;
5. Brain tumor classification:
while *t* < *tmax* do
Initialize ensemble of DCLSTM models with different hyperparameters;
Train each DCLSTM model with extracted feature sequence; *// Training phase*
Learn the spatial and temporal information;
Classification phase:
For an input image a:
Predict tumor class (vote);
End for;
Accumulate votes of each model in the ensemble;
Apply majority voting;
Select a class with maximum voting;
t++;
End while;
End

Results and discussion

For the purpose of precisely classifying brain cancers, this team built a hybrid deep-learning architecture. On a Windows 7 computer, the Python platform was used to model and implement the suggested EL-DCLSTM. Accuracy, precision, recall (sensitivity), f-measure, specificity, false positive rate (FPR), and false negative rate (FNR) are used to evaluate the proposed algorithm's performances.

Performance Assessment

This section evaluated the suggested strategy's performance in terms of accuracy and loss. First, the input database was divided into training and validation ratios of 70:30. The suggested EL-DCLSTM model was trained on the training set to help it recognize patterns in the data that would help classify brain tumors. On the other hand, new samples (those not included in the training set) are utilized in the validation set to evaluate how well the produced algorithm performs. The accuracy for both the training and validation sets is shown in Figure 4. The model's learning efficiency—or how well it recognizes patterns and correlations in the data to forecast brain tumors—is determined by its training accuracy. The proposed algorithm's prediction accuracy on fresh or unidentified samples is measured by the validation accuracy. The accuracy of the validation and training was evaluated by increasing the number of epochs from 0 to 14.

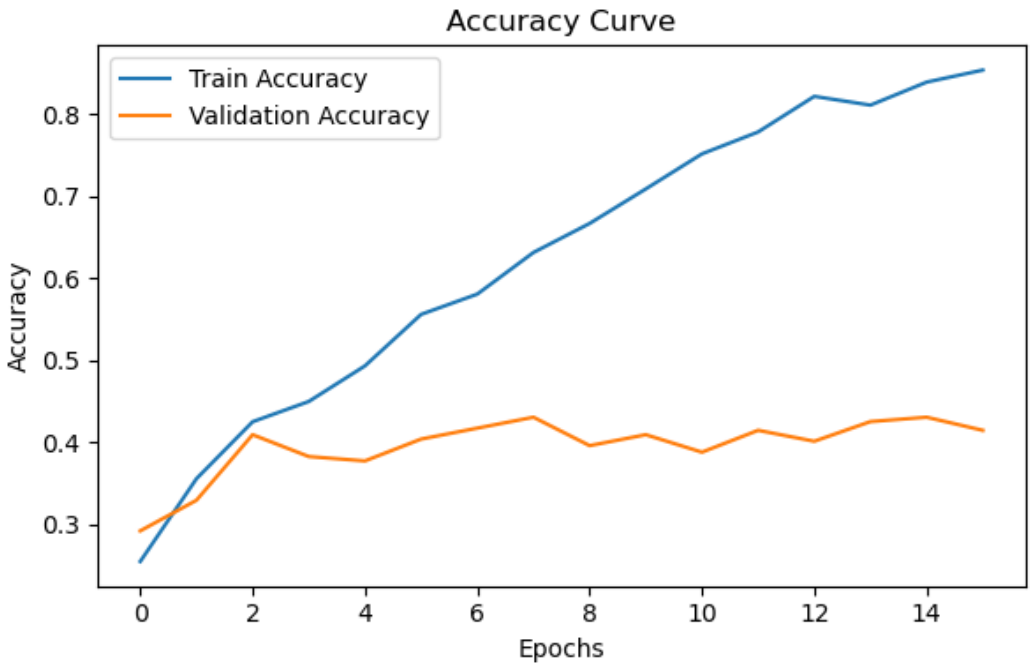

Figure 4: Accuracy analysis

This research demonstrates that the accuracy of the suggested approach grew with the number of epochs and reached a higher level during the training period (0.9). However, the created algorithm only managed to accomplish about 0.4%, indicating that the system is not very good at predicting the classifications of brain tumors on unidentified samples.

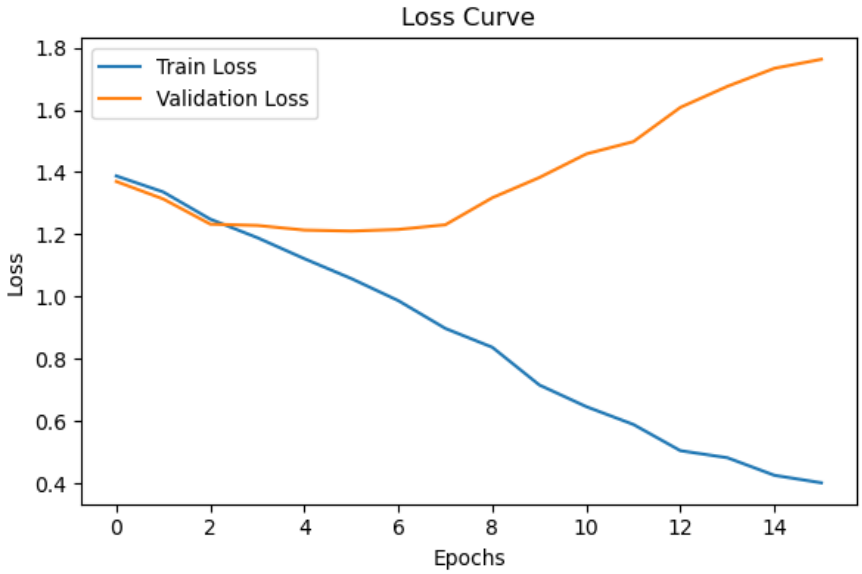

Figure 5: Loss analysis

To ascertain the classification error, the loss was assessed during both the training and validation stages. The difference between the actual and anticipated brain tumor class is measured by the loss or error rate. If the anticipated class and actual class coincide, there will be little loss. Figure 5 shows the analysis of the loss. The validation loss shows how well the model predicts the various kinds of brain tumors, whereas the training loss measures the inaccuracy during the training phase. The model's training loss diminishes over the course of the epochs, demonstrating the dependability and efficiency of the system in picking up tumor pattern recognition. But as epochs go by, the model's validation loss rises, indicating that the established technique is not able to generalize successfully to previously unknown data sets.

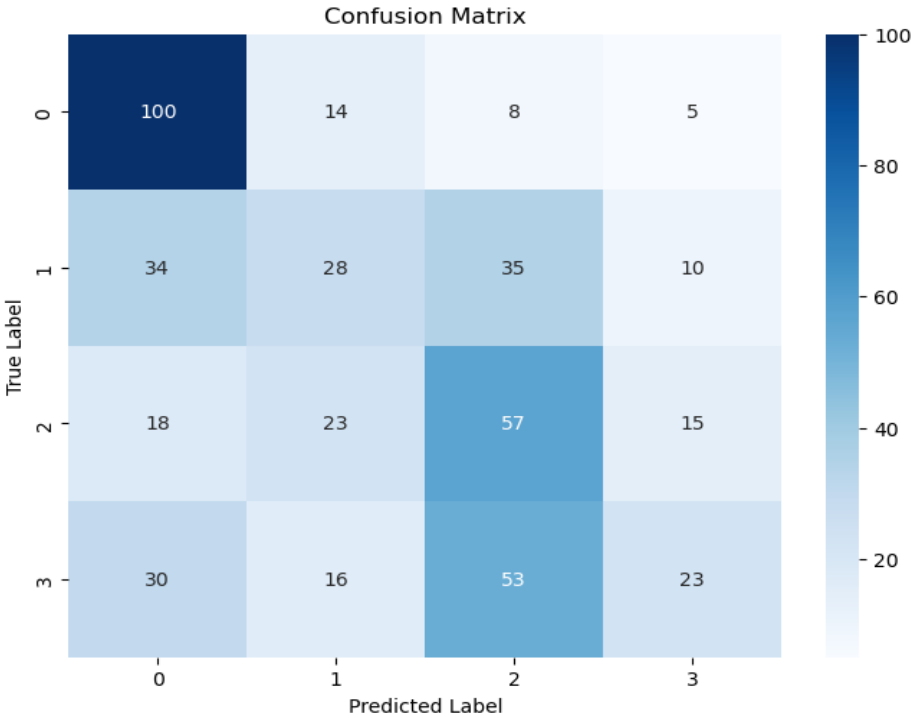

Figure 6: Confusion Matrix

A table that is used to gauge the classification model's performance is represented by a confusion matrix. It assesses the degree to which the suggested approach distinguishes between various classes within the dataset. The model's performance is assessed by the confusion matrix using four distinct metrics: true positive (TP), true negative (TN), false positive (FP), and false negative (FN). When both the actual and predicted classes belong to the positive class, the proposed model successfully classifies positive cases; this is the scenario denoted by TP. TN stands for the scenarios in which the model accurately forecasts the negative occurrences.

Conversely, FP characterizes the situation in which the model misclassifies the negative occurrence as positive. Simultaneously, FN represents the situation in which the model misidentifies the positive instance as negative. We are able to interpret the efficacy (both strength and weakness) in completing tasks related to brain tumor classification thanks to this thorough evaluation. This is the confusion matrix in Figure 6.

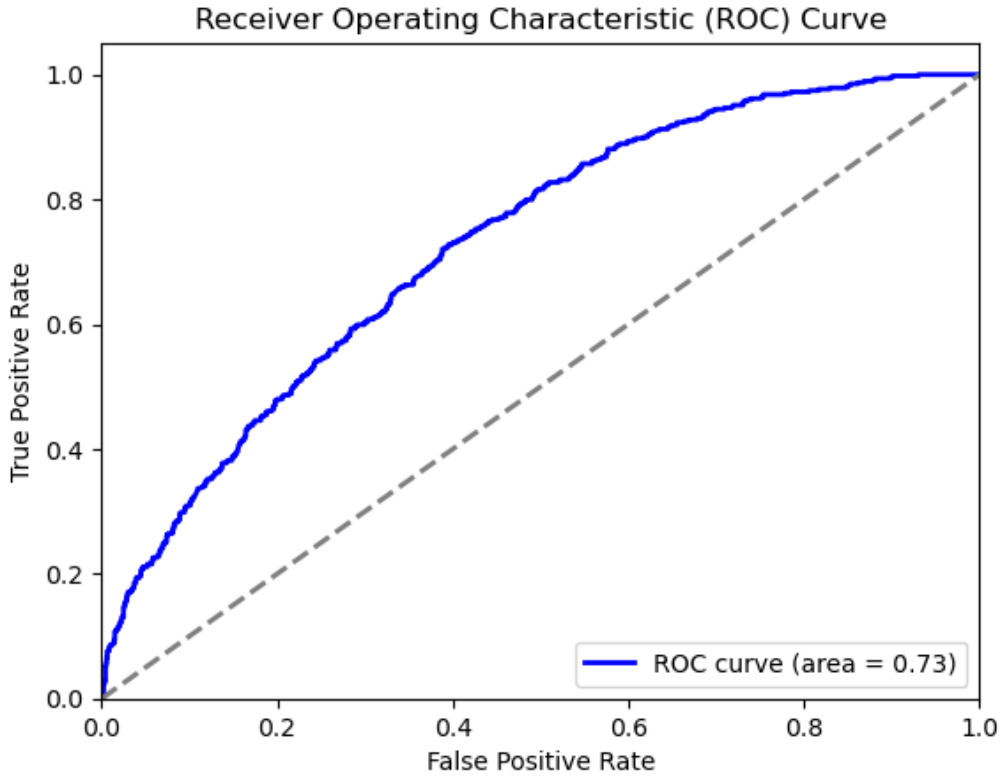

Figure 7: ROC curve

The ROC curve, which offers a thorough summary of the trade-offs between specificity and sensitivity, is the graphical representation used to measure the classification performance of the system. At various categorization criteria, it shows the true positive rate against the false positive rate. The ROC curve is shown in Figure 7. By calculating an Area Under the Curve (AUC), it assesses the categorization ability. With an AUC of 0.73, the established method has a 73% likelihood of accurately differentiating brain tumor classifications.

Evaluation metrics

The parameters utilized to assess the developed algorithm's performance in classifying brain tumors are covered in this section.

The following measures are used to assess performance: f-measure, FPR, FNR, accuracy, precision, sensitivity, and specificity. Below is a definition and calculation for these measurements.

Accuracy:The model's accuracy quantifies how well it can classify various types of brain tumors. It is expressed in Eqn and defines the proportion of correctly classified cases to all instances. (17).

$$Accuracy = \left(\frac{Tp^{+} + Tn^{-}}{Tp^{+} + Tn^{-} + Fp^{+} + Fn^{-}} \right) \quad (17)$$

Where Tp^{+}, Tn^{-}, Fp^{+} and Fn^{-} indicates TP, TN, FP, and FN, respectively.

Precisin:

The precision of the model is a measure of how well it detects genuine positive cases. It defines the ratio of actual positive cases to all positive cases, as given by Equation. (18).

$$\Pr ecision = \left(\frac{Tp^{+}}{Tp^{+} + Fp^{+}} \right) \quad (18)$$

Sensitivity:

The sensitivity, sometimes referred to as recall, gauges how well the model can locate pertinent examples. It is represented

in Eqn and shows the ratio of real positives that the model correctly identifies. (19).

$$Sensitivity = \left(\frac{Tp^{+}}{Tp^{+} + Fn^{-}} \right) \quad (19)$$

F-measure:

The harmonic mean of recall and precision metrics is defined by the F-measure. This measure, which is established mathematically in Eqn, provides a fair assessment of the model's performance taking into account both positive and negative examples.(20).

$$F - measure = 2 \times \left(\frac{\mathrm{Re}\,call * \mathrm{Pr}\,ecision}{\mathrm{Re}\,call + \mathrm{Pr}\,ecision} \right) \quad (20)$$

Specificity:

he model's specificity indicates how well it detects actual negative cases. It is theoretically represented in Eqn and defines the ratio of real negative examples successfully identified by the suggested model. (21).

$$Specificity = \left(\frac{Tn^{-}}{Tn^{-} + Fp^{+}} \right) \quad (21)$$

False positive rate:

Formulated in Eqn, FPR represents the ratio of actual negatives that the classifier mistakenly predicts as positives. (22).

$$FPR = \left(\frac{Fp^{+}}{Tn^{-} + Fp^{+}} \right) \quad (22)$$

False negative rate:

FNR, as given in Eqn, is the ratio of real positive cases that the devised algorithm mistakenly forecasted as negatives. (23).

$$FNR = \left(\frac{Fn^{-}}{Tp^{+} + Fn^{-}} \right) \quad (23)$$

Evaluation of these metrics enables us to determine the efficiency of the developed model in classifying different classes of brain tumors.

Comparative assessment

This part served to validate the efficacy and dependability of the suggested technique for classifying brain tumors by comparing its performance to that of the current models. Deep Convolutional Neural Networks (DCNNs) are among the traditional models utilized for comparative evaluation.

[37], Recurrent Neural Network with Long Short Term Memory (RNN-LSTM) [38], Convolutional Neural Network integrated with Long Short Term Memory (CNN-LSTM) [39], Attention-based Recurrent Neural Network (Ab-RNN) [40], and Deep Belief Network (DBN) [41]. The following metrics are employed in comparative analysis: f-measure, FPR, FNR, accuracy, precision, sensitivity, and specificity. The effectiveness of the current models and suggested approach is assessed by running them on the Python platform and evaluating them using the same dataset as the study that is being presented. Also, the performances are evaluated in two cases: (1) splitting the dataset in an 80:20 ratio and (2) splitting the dataset in a 70:30 ratio.

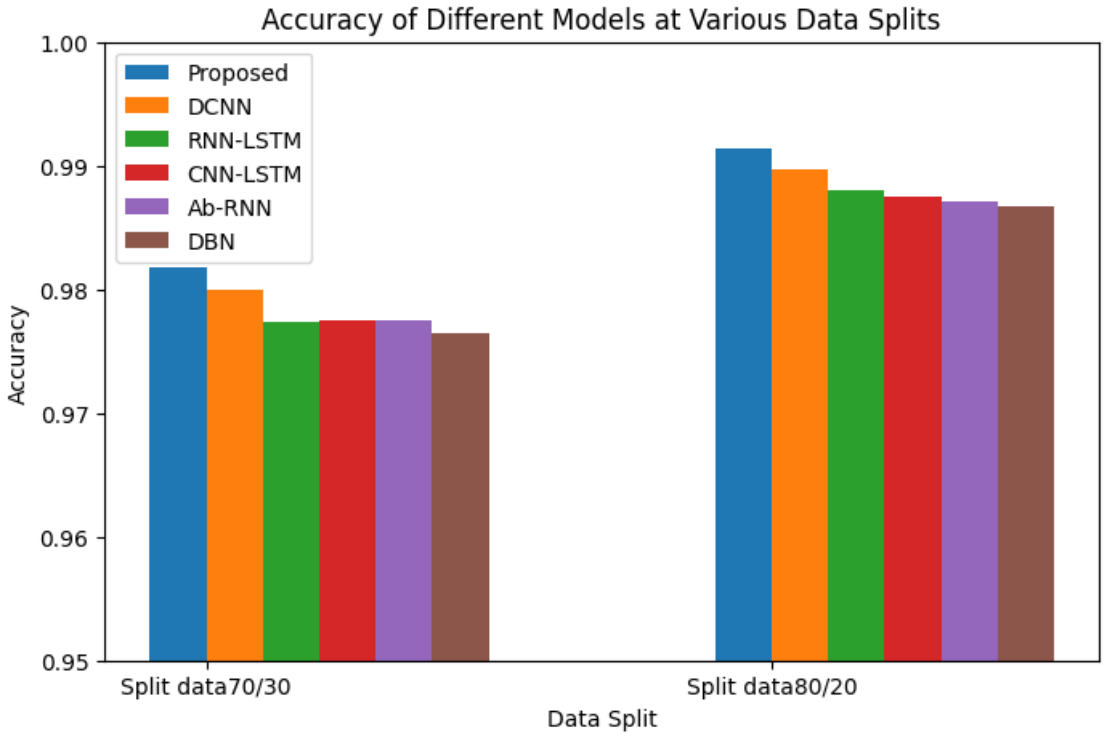

Figure 8: Accuracy comparison

The accuracy statistic assesses how accurately the model has classified the various tumor classifications overall. The accuracy of the traditional techniques (DBN, Ab-RNN, CNN-LSTM, RNN-LSTM, and DCNN) for 70/30 data split was 0.97652, 0.97752, 0.97752, 0.97738, and 0.97993, in that order. Conversely, the algorithm that was built managed to attain a higher accuracy of 0.98172. The suggested technique achieved a greater accuracy of 0.99138 for the 80/20 data split than the current models, which included DBN, Ab-RNN, CNN-LSTM, RNN-LSTM, and DCNN, which earned accuracy rates of 0.98670, 0.98712, 0.98755, 0.98797, and 0.98967, respectively. Figure 8 shows the accuracy contrast. It is clear from this analysis that the suggested method outperformed the current models in terms of accuracy. Furthermore, a high training ratio is shown to enhance the accuracy of the system, indicating that training with vast amounts of data facilitates comprehension of the complex patterns included in the data.

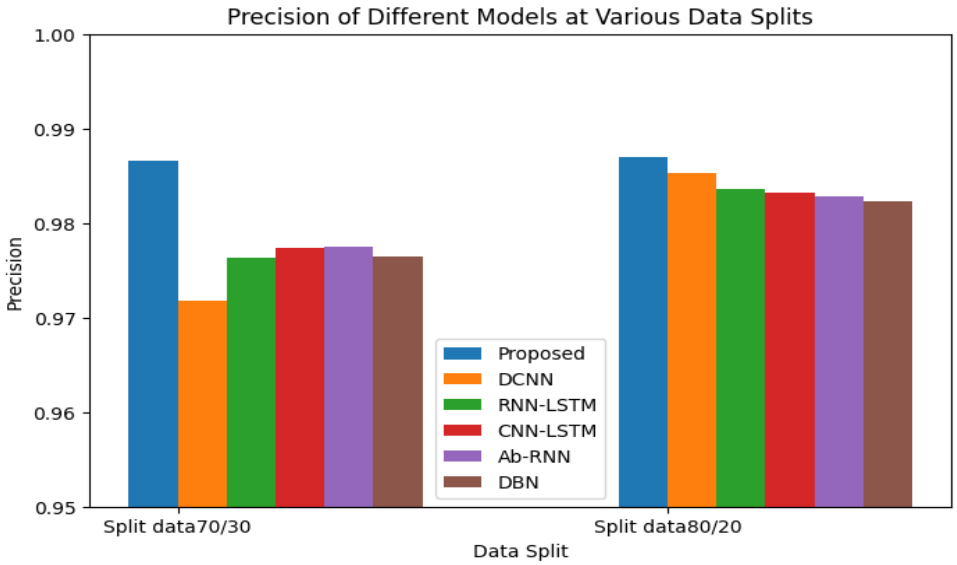

Figure 9: Precision comparison

The accuracy of the model's predictions of the positive cases is determined by its precision. Figure 9 shows the precision comparison. The suggested strategy achieved increased precision of 0.98664, while the currently available approaches, including DBN, Ab-RNN, CNN-LSTM, RNN-LSTM, and DCNN, earned precision of 0.97672, 0.97752, 0.97735, 0.97628, and 0.97172, respectively, for 70/30 data split. Conversely, the traditional models (DBN, Ab-RNN, CNN-LSTM, RNN-LSTM, and DCNN) obtained a precision of 0.98234, 0.98276, 0.98318, 0.98361, and 0.98531 with an 80/20 data split. Nevertheless, the suggested technique achieved a higher precision of 0.98701. This precision evaluation shows that the developed algorithm outperformed other methods in terms of precision, demonstrating its dependability and effectiveness in detecting and categorizing positive cases.

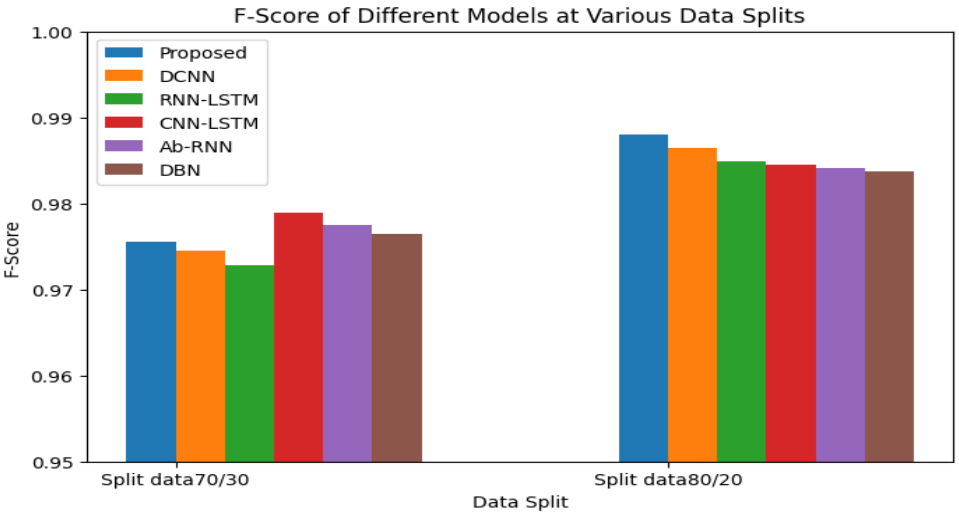

Figure 10: F1-score comparison

The F-measure, also known as the F1-score, provides a balanced system performance by defining the harmonic mean of precision and recall. The comparison of the f-measure is shown in Figure 10. The current algorithms, including DBN, Ab-RNN, CNN-LSTM, RNN-LSTM, and DCNN, obtained f1-scores of 0.97562, 0.97752, 0.97898, 0.97288, and 0.97455 for 70/30 data split, in that order. Nonetheless, the framework that was presented achieved a higher f1-score of 0.98172. The suggested framework produced an improved f-measure of 0.98805, while the above-stated strategies obtained f-measures of 0.98374, 0.98413, 0.98452, 0.98491, and 0.98648, respectively, for the 80/20 data split. According to this comparative analysis of the f-measure, the suggested method offers a balanced classification performance that takes into account both positive and negative cases. Furthermore, it is seen that the models had better results with a higher training ratio, indicating that training on a big dataset improves classification performances.

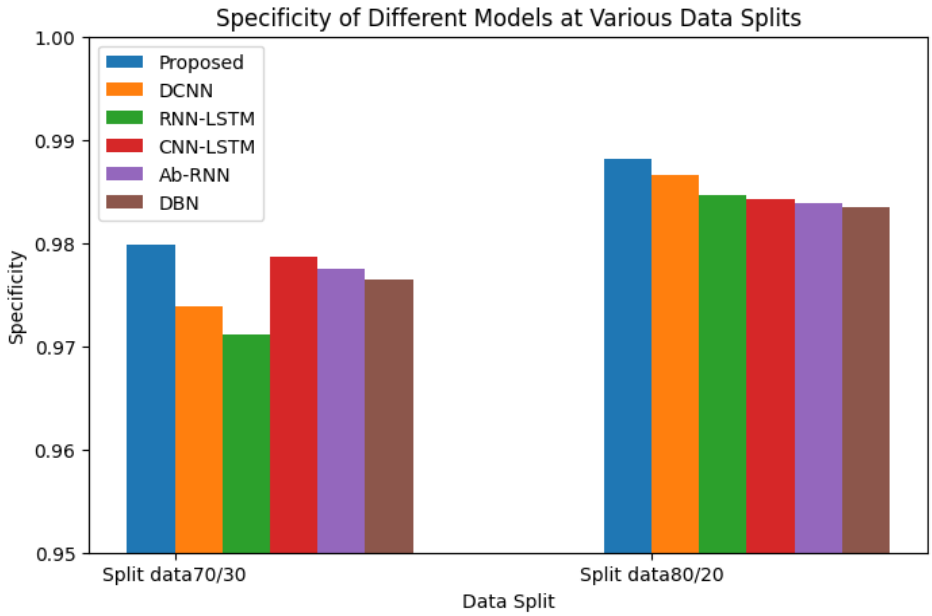

Figure 11: Specificity comparison

The model's specificity governs its capacity to recognize and categorize actual negative cases. The comparison of specificity is shown in Figure 11. The new approach produced a higher f1-score of 0.97983, whereas the previously mentioned existing models obtained specificities of 0.97652, 0.97652, 0.97864, 0.97113, and 0.97381, respectively, for 70/30 data split. Conversely, the traditional algorithms, such as DBN, Ab-RNN, CNN-LSTM, RNN-LSTM, and DCNN, obtained specificity of 0.98345, 0.98383, 0.98422, 0.98461, and 0.98656, with an 80/20 data split. The new method, however, achieved a better specificity of 0.98812. When compared to the current models, the suggested method accurately predicts and classifies the genuine negative instances, as evidenced by the notable improvement in the specificity rate.

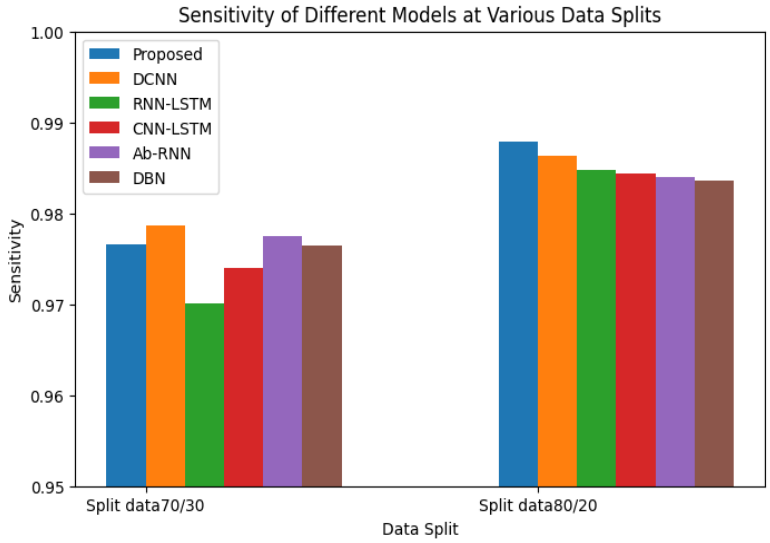

Figure 12: Sensitivity comparison

The system's ability to recognize and classify real positive cases among all positive instances is measured by sensitivity or recall. The aforementioned existing methodologies achieved sensitivity values of 0.97652, 0.97254, 0.97395, 0.97009, and 0.97866, respectively, for a 70/30 data split. Conversely, the method that was built managed to attain a higher sensitivity of 0.97954. The created technique achieved a higher sensitivity of 0.98793 for the 80/20 data split, compared to the above-stated conventional models that earned sensitivity of 0.98358, 0.98397, 0.98437, 0.98476, and 0.98635, respectively. The sensitivity comparison is shown in Figure 12. The suggested framework's increased sensitivity demonstrates its dependability and efficiency in accurately categorizing positive cases. This confirms that the suggested model makes accurate classification when compared to other models that are already accessible.

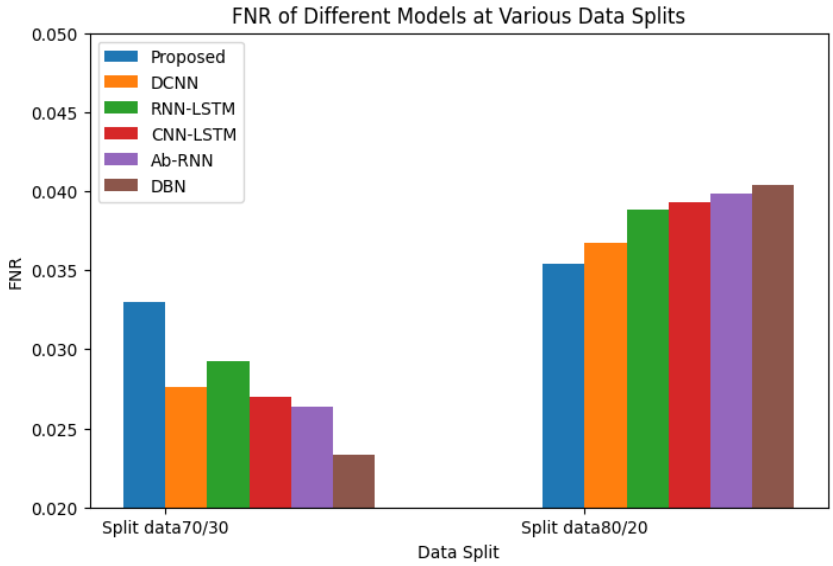

Figure 13: FNR comparison

By calculating the total number of inaccurate classifications the system has made, the FNR measure calculates the false prediction rate produced by the model. Figure 13 shows the comparison of FNR. The new technique obtained least FNR of 0.03296, while the existing models, namely DBN, Ab-RNN, CNN-LSTM, RNN-LSTM, and DCNN, earned FNR of 0.02333, 0.02639, 0.02698, 0.02924, and 0.02758, respectively, for 70/30 data split. On the other hand, for an 80/20 data split, the traditional techniques such as DBN, Ab-RNN, CNN-LSTM, RNN-LSTM, and DCNN obtained FNR of 0.03000, 0.02970, 0.02941, 0.02913, and 0.02778, respectively. However, the designed algorithm earned a reduced FNR of 0.02655. The significant reduction of FNR in the developed algorithm manifests its efficiency in preventing false negative predictions.

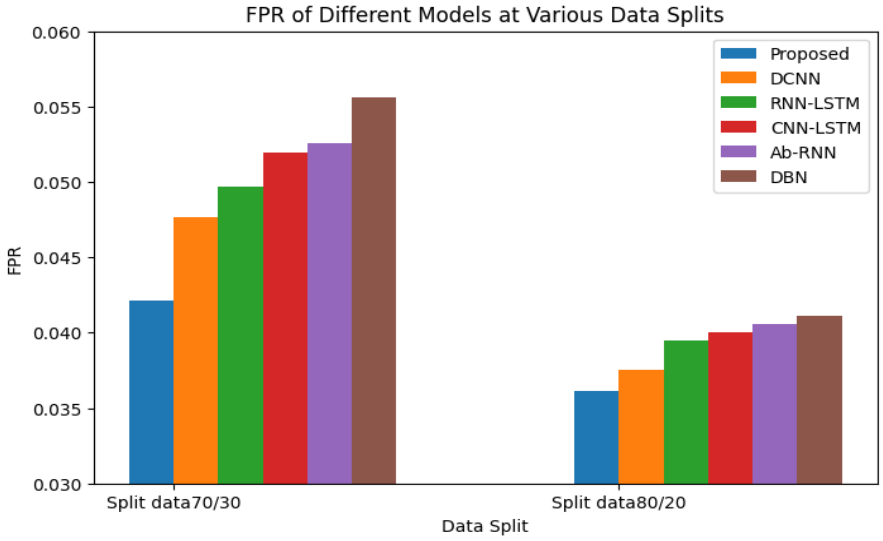

Figure 14: FPR comparison

The model's erroneous prediction is measured by the FPR. It assesses the proportion of falsely detected negative cases. The FPR of the existing methods, such as DBN, Ab-RNN, CNN-LSTM, RNN-LSTM, and DCNN, for a 70/30 data split was 0.05562, 0.05257, 0.05198, 0.04972, and 0.044765, in that order. The created technique, however, achieved a minimal FPR of 0.04216. The FPR for the 80/20 data split was obtained by the current models, which include DCNN, Ab-RNN, CNN-LSTM, 0.03947, 0.04054, and 0.04110, respectively. The developed method did, however, receive a minimal FPR of 0.03614. Figure 14 shows the FPR comparison. The developed algorithm's effectiveness in preventing incorrect predictions is demonstrated by the notable decrease in false positive rate (FPR). This further demonstrates how precisely the suggested algorithm categorizes the negative cases. This thorough comparative analysis demonstrates that the suggested approach produced better outcomes in terms of f-measure, sensitivity, specificity, accuracy, and precision.

Discussion

In order to effectively classify the various tumor classifications, a novel hybrid model was presented. The paradigm that is being presented combines the benefits of group learning with DCLSTM. The multiple tumor class BraTs 2020 dataset, which is publically available, was employed in the proposed methodology. After preprocessing the raw dataset, the region of interest was found by image segmentation. As a result, an enhanced version of the ResNet technique was used for feature extraction, capturing the most important features necessary for distinguishing between the various tumor types.

Table 1: Comparative evaluation of different models at 80/20 data split

Metrics	DBN	Ab-RNN	CNN-LSTM	RNN-LSTM	DCNN	Proposed
Accuracy	0.98670	0.98712	0.98755	0.98797	0.98967	0.99138
Precision	0.98234	0.98276	0.98318	0.98361	0.98531	0.98701
F1-Score	0.98374	0.98413	0.98452	0.98491	0.98648	0.98805
Specificity	0.98345	0.98383	0.98422	0.98461	0.98656	0.98812
Sensitivity	0.98358	0.98397	0.98437	0.98476	0.98635	0.98793
FPR	0.04110	0.04054	0.04000	0.03947	0.03750	0.03614
FNR	0.03000	0.02970	0.02941	0.02913	0.02778	0.02655

Finally, multiclass tumor categorization was performed using the proposed EL-DCLSTM after intensive training using extracted features. Multiple DCLSTM were created with different hyperparameter values and trained using feature subsets obtained from the feature extraction module. The ensemble learning aggregates each DCLSTM's predictions, producing final classification results. The proposed framework was executed in the Python platform, and the results are determined as accuracy, precision, sensitivity, specificity, f1-score, FPR, and FNR at two different data splits (70/30 and 80/20).

Table 2: Comparative evaluation of different models at 70/30 data split

Metrics	DBN	Ab-RNN	CNN-LSTM	RNN-LSTM	DCNN	Proposed
Accuracy	0.97652	0.97752	0.97752	0.97738	0.97993	0.98172
Precision	0.97672	0.97752	0.97735	0.97628	0.97172	0.98664
F1-Score	0.97562	0.97752	0.97898	0.97288	0.97455	0.98557
Specificity	0.97652	0.97652	0.97864	0.97113	0.97381	0.97983
Sensitivity	0.97254	0.97275	0.97395	0.97009	0.97866	0.97954
FPR	0.05562	0.05257	0.05198	0.04972	0.044765	0.04216
FNR	0.02333	0.02639	0.02698	0.02924	0.02758	0.03296

Moreover, a comparative analysis was carried out to verify the efficacy of the proposed framework in tumor classification against established models including DBN, Ab-RNN, CNN-LSTM, RNN-LSTM, and DCNN. Tables 1 and 2 present a comparative evaluation of the performance of several models. This assessment shows that the suggested approach achieved higher scores on measures such as f-measure, sensitivity, specificity, accuracy, and precision. On the other hand, the parameters like FPR and FNR are reduced in the presented algorithm compared to the currently existing models. These improved performances highlight the efficiency of the developed framework in tumor classification. Thus, the combination of ensemble learning and DCLSTM offers improved tumor categorization.

Conclusion

In order to classify brain tumors into multiple classes, this work proposed a hybrid deep learning model that combined the advantages of ensemble learning and deep convolutional long short term memory. The approach that was provided employed a Gaussian filter to exclude undesirable features and noise from the images. The required properties are then extracted and segmented from the preprocessed images using enhanced U-Net and ResNet algorithms. The BraTs 2020 database was used to validate the Python software that implemented the described framework.

The experimental findings show that for 70% and 80% of the training data, the suggested technique produced greater accuracy of 0.98664 and 0.99138.

Additionally, 0.98867 precision, 0.98123 f1-score, 0.97954 specificity, 0.97954 sensitivity, 0.04216 FPR, and 0.03296 FNR were all averaged by the suggested algorithm. Ultimately, a thorough compared analysis was conducted between the outcomes of the suggested approach and those of other models, including DBN, Ab-RNN, CNN-LSTM, RNN-LSTM, and DCNN. The comparative analysis demonstrated that, in comparison to the current methods, the suggested strategy provided better results in terms of accuracy, specificity, sensitivity, f1-score, and precision. Despite achieving better classification performances, the new method has some drawbacks. First off, the suggested algorithm's performance in actual clinical circumstances is constrained by its limited applicability towards the validation sequence. Second, because the study's scalability was not examined using a variety of datasets, there was still cause for concern. Thirdly, ensemble learning imposes computational complexity on classification tasks. In the future, these issues must be resolved by creating an optimum classification method that combines multi-objective optimization and deep learning techniques.

References

Ahamed, Jisan, BH Jaswanth Gowda, Waleed H. Almalki, Neelima Gupta, Amirhossein Sahebkar, and Prashant Kesharwani. "Recent advances in nanoparticle-based approaches for the treatment of brain tumors: Opportunities and challenges." European Polymer Journal 193 (2023): 112111.

Bhuiya, Nabila. "A review on the occurrence of brain tumor in adults and pediatrics and the associated risk factors." PhD diss., Brac University, 2023.

Fanous, Eng Ereny Magdy Abdelmalak. "Deep Learning Based CAD System for Early Detection of Brain Tumor." PhD diss., Benha University, 2024.

Rela, Munipraveena, Nagaraja Rao Suryakari, and Ramana Reddy Patil. "A diagnosis system by U-net and deep neural network enabled with optimal feature selection for liver tumor detection using CT images." Multimedia Tools and Applications 82, no. 3 (2023): 3185-3227.

Frosina, Guido. "Recapitulating the key advances in the diagnosis and prognosis of high-grade gliomas: second half of 2021 update." International Journal of Molecular Sciences 24, no. 7 (2023): 6375.

Ahamed, Jisan, BH Jaswanth Gowda, Waleed H. Almalki, Neelima Gupta, Amirhossein Sahebkar, and Prashant Kesharwani. "Recent advances in nanoparticle-based approaches for the treatment of brain tumors: Opportunities and challenges." European Polymer Journal 193 (2023): 112111.

Miller, Braden, Hunter Chalfant, Alexandra Thomas, Elizabeth Wellberg, Christina Henson, Molly W. McNally, William E. Grizzle, Ajay Jain, and Lacey R. McNally. "Diabetes, obesity, and inflammation: impact on clinical and radiographic features of breast cancer." International journal of molecular sciences 22, no. 5 (2021): 2757.

De Ruysscher, Dirk, Corinne Faivre-Finn, K. Nackaerts, K. Jordan, J. Arends, Jean-Yves Douillard, Umberto Ricardi, and S. Peters. "Recommendation for supportive care in patients receiving concurrent chemotherapy and radiotherapy for lung cancer." Annals of Oncology 31, no. 1 (2020): 41-49.

Fernandes, Steven Lawrence, U. John Tanik, V. Rajinikanth, and K. Arvind Karthik. "A reliable framework for accurate brain image examination and treatment planning based on early diagnosis support for clinicians." Neural Computing and Applications 32, no. 20 (2020): 15897-15908.

Zhou, S. Kevin, Hayit Greenspan, Christos Davatzikos, James S. Duncan, Bram Van Ginneken, Anant Madabhushi, Jerry L. Prince, Daniel Rueckert, and Ronald M. Summers. "A review of deep learning in medical imaging: Imaging traits, technology trends, case studies with progress highlights, and future promises." Proceedings of the IEEE 109, no. 5 (2021): 820-838.

Aamir, M., Rahman, Z., Dayo, Z. A., Abro, W. A., Uddin, M. I., Khan, I., ... & Hu, Z. (2022). A deep learning approach for brain tumor classification using MRI images. Computers and Electrical Engineering, 101, 108105.

Mzoughi, Hiba, Ines Njeh, Mohamed Ben Slima, Ahmed Ben Hamida, Chokri Mhiri, and Kheireddine Ben Mahfoudh. "Towards a computer aided diagnosis (CAD) for brain MRI glioblastomas tumor exploration based on a deep convolutional neuronal networks (D-CNN) architectures." Multimedia Tools and Applications 80 (2021): 899-919.

Kadhim, Yezi Ali, Muhammad Umer Khan, and Alok Mishra. "Deep learning-based computer-aided diagnosis (cad): applications for medical image datasets." Sensors 22, no. 22 (2022): 8999.

Tasci, Burak, and Irem Tasci. "Deep feature extraction based brain image classification model using preprocessed images: PDRNet." Biomedical Signal Processing and Control 78 (2022): 103948.

Kumar, Dharmender. "Feature extraction and selection of kidney ultrasound images using GLCM and PCA." Procedia Computer Science 167 (2020): 1722-1731.

Beeravolu, Abhijith Reddy, Sami Azam, Mirjam Jonkman, Bharanidharan Shanmugam, Krishnan Kannoorpatti, and Adnan Anwar. "Preprocessing of breast cancer images to create datasets for deep-CNN." IEEE Access 9 (2021): 33438-33463.

Macedo, Mariana, Maira Santana, Wellington P. dos Santos, Ronaldo Menezes, and Carmelo Bastos-Filho. "Breast cancer diagnosis using thermal image analysis: A data-driven approach based on swarm intelligence and supervised learning for optimized feature selection." Applied Soft Computing 109 (2021): 107533.

Sahoo, Limali, Lokanath Sarangi, Bidyut Ranjan Dash, and Hemanta Kumar Palo. "Detection and classification of brain tumor using magnetic resonance images." In Advances in Electrical Control and Signal Systems: Select Proceedings of AECSS 2019, pp. 429-441. Springer Singapore, 2020.

Qureshi, Shahzad Ahmad, Shan E. Ahmed Raza, Lal Hussain, Areej A. Malibari, Mohamed K. Nour, Aziz ul Rehman, Fahd N. Al-Wesabi, and Anwer Mustafa Hilal. "Intelligent ultra-light deep learning model for multiclass brain tumor detection." Applied Sciences 12, no. 8 (2022): 3715.

Waqas, Asim, Dimah Dera, Ghulam Rasool, Nidhal Carla Bouaynaya, and Hassan M. Fathallah-Shaykh. "Brain tumor segmentation and surveillance with deep artificial neural networks." Deep Learning for Biomedical Data Analysis: Techniques, Approaches, and Applications (2021): 311-350.

Solanki, Shubhangi, Uday Pratap Singh, Siddharth Singh Chouhan, and Sanjeev Jain. "Brain tumor detection and classification using intelligence techniques: an overview." IEEE Access 11 (2023): 12870-12886.

Badža, Milica M., and Marko Č. Barjaktarović. "Classification of brain tumors from MRI images using a convolutional neural network." Applied Sciences 10, no. 6 (2020): 1999.

Jabbar, Ayesha, Shahid Naseem, Tariq Mahmood, Tanzila Saba, Faten S. Alamri, and Amjad Rehman. "Brain tumor detection and multi-grade segmentation through hybrid caps-VGGNet model." IEEE Access 11 (2023): 72518-72536.

Sharif, Muhammad Imran, Muhammad Attique Khan, Musaed Alhussein, Khursheed Aurangzeb, and Mudassar Raza. "A decision support system for multimodal brain tumor classification using deep learning." Complex & Intelligent Systems (2021): 1-14.

Kumar, Sandeep, Shilpa Choudhary, Arpit Jain, Karan Singh, Ali Ahmadian, and Mohd Yazid Bajuri. "Brain tumor classification using deep neural network and transfer learning." Brain topography 36, no. 3 (2023): 305-318.

Asif, Sohaib, Ming Zhao, Fengxiao Tang, and Yusen Zhu. "An enhanced deep learning method for multiclass brain tumor classification using deep transfer learning." Multimedia Tools and Applications 82, no. 20 (2023): 31709-31736.

Emam, Marwa M., Nagwan Abdel Samee, Mona M. Jamjoom, and Essam H. Houssein. "Optimized deep learning architecture for brain tumor classification using improved Hunger Games Search Algorithm." Computers in Biology and Medicine 160 (2023): 106966.

Tabatabaei, Sadafossadat, Khosro Rezaee, and Min Zhu. "Attention transformer mechanism and fusion-based deep learning architecture for MRI brain tumor classification system." Biomedical Signal Processing and Control 86 (2023): 105119.

Mehnatkesh, Hossein, Seyed Mohammad Jafar Jalali, Abbas Khosravi, and Saeid Nahavandi. "An intelligent driven deep residual learning framework for brain tumor classification using MRI images." Expert Systems with Applications 213 (2023): 119087.

Krishnapriya, Srigiri, and Yepuganti Karuna. "A survey of deep learning for MRI brain tumor segmentation methods: Trends, challenges, and future directions." Health and Technology 13, no. 2 (2023): 181-201.

BraTs 2020 dataset accessible at https://www.med.upenn.edu/cbica/brats2020/data.html.

Akter, Atika, Nazeela Nosheen, Sabbir Ahmed, Mariom Hossain, Mohammad Abu Yousuf, Mohammad Ali Abdullah Almoyad, Khondokar Fida Hasan, and Mohammad Ali Moni. "Robust clinical applicable CNN and U-Net based algorithm for MRI classification and segmentation for brain tumor." Expert Systems with Applications 238 (2024): 122347.

Periasamy, J. K., S. Buvana, and P. Jeevitha. "Comparison of VGG-19 and RESNET-50 Algorithms in Brain Tumor Detection." In 2023 IEEE 8th International Conference for Convergence in Technology (I2CT), pp. 1-5. IEEE, 2023.

Behrad, Fatemeh, and Mohammad Saniee Abadeh. "Evolutionary convolutional neural network for efficient brain tumor segmentation and overall survival prediction." Expert Systems with Applications 213 (2023): 118996.

Neeraja, K., B. Madhavi, Ch Kavya, and R. Sankeerthana. "Brain Tumor Detection Using Long Short Term Memory." In 2023 International Conference on Research Methodologies in Knowledge Management, Artificial Intelligence and Telecommunication Engineering (RMKMATE), pp. 1-7. IEEE, 2023.

Khan, Farhana, Shahnawaz Ayoub, Yonis Gulzar, Muneer Majid, Faheem Ahmad Reegu, Mohammad Shuaib Mir, Arjumand Bano Soomro, and Osman Elwasila. "MRI-based effective ensemble frameworks for predicting human brain tumor." Journal of Imaging 9, no. 8 (2023): 163.

Alyami, Jaber, Amjad Rehman, Fahad Almutairi, Abdul Muiz Fayyaz, Sudipta Roy, Tanzila Saba, and Alhassan Alkhurim. "Tumor localization and classification from MRI of brain using deep convolution neural network and Salp swarm algorithm." Cognitive Computation 16, no. 4 (2024): 2036-2046.

Vallathan, G., Venkata Rao Yanamadni, R. G. Vidhya, Ananda Ravuri, C. Ambhika, and V. V. S. Sasank. "An analysis and study of brain cancer with RNN algorithm based AI technique." In 2023 7th International Conference on I-SMAC (IoT in Social, Mobile, Analytics and Cloud)(I-SMAC), pp. 637-642. IEEE, 2023.

Gómez-Guzmán, Marco Antonio, Laura Jiménez-Beristaín, Enrique Efren García-Guerrero, Oscar Roberto López-Bonilla, Ulises Jesús Tamayo-Perez, José Jaime Esqueda-Elizondo, Kenia Palomino-Vizcaino, and Everardo Inzunza-González. "Classifying brain tumors on magnetic resonance imaging by using convolutional neural networks." Electronics 12, no. 4 (2023): 955.

Saurav, Sumeet, Ayush Sharma, Ravi Saini, and Sanjay Singh. "An attention-guided convolutional neural network for automated classification of brain tumor from MRI." Neural Computing and Applications 35, no. 3 (2023): 2541-2560.

Mahmud, Md Ishtyaq, Muntasir Mamun, and Ahmed Abdelgawad. "A deep analysis of brain tumor detection from mr images using deep learning networks." Algorithms 16, no. 4 (2023): 176.